





Article

Palladium Nanoparticles on Chitosan-Coated Superparamagnetic Manganese Ferrite: A Biocompatible Heterogeneous Catalyst for Nitroarene Reduction and Allyl Carbamate Deprotection

Mona Ebadi ¹, Nurul Asikin-Mijan ¹, Mohd Suzeren Md. Jamil ¹, Anwar Iqbal ², Emad Youisif ³, Ahmad Rifqi Md Zain ^{4,*}, Tengku Hasnan Tengku Aziz ⁴ and Muhammad Rahimi Yusop ^{1,*}

¹ Department of Chemical Sciences, Faculty of Science and Technology, Universiti Kebangsaan Malaysia (UKM), Bangi 43600, Selangor, Malaysia

² School of Chemical Sciences, Universiti Sains Malaysia, Penang 11800, Malaysia

³ Department of Chemistry, College of Science, Al-Nahrain University, Baghdad 64074, Iraq

⁴ Institute of Microengineering and Nanoelectronics (IMEN), Universiti Kebangsaan Malaysia (UKM), Bangi 43600, Selangor, Malaysia

* Correspondence: rifqi@ukm.edu.my (A.R.M.Z.); rahimi@ukm.edu.my (M.R.Y.);

Tel.: +603-89118160 (A.R.M.Z.); +60-10-2678586 (M.R.Y.)

Abstract: Although metallic nanocatalysts such as palladium nanoparticles (Pd NPs) are known to possess higher catalytic activity due to their large surface-to-volume ratio, however, in nano-size greatly reducing their activity due to aggregation. To overcome this challenge, superparamagnetic chitosan-coated manganese ferrite was successfully prepared and used as a support for the immobilization of palladium nanoparticles to overcome the above-mentioned challenge. The Pd-Chit@MnFe₂O₄ catalyst exhibited high catalytic activity in 4-nitrophenol and 4-nitroaniline reductions, with respective turnover frequencies of 357.1 min⁻¹ and 571.4 min⁻¹, respectively. The catalyst can also be recovered easily by magnetic separation after each reaction. Additionally, the Pd-Chit@MnFe₂O₄ catalyst performed well in the reductive deprotection of allyl carbamate. Coating the catalyst with chitosan reduced the Pd leaching and its cytotoxicity. Therefore, the catalytic activity of Pd-Chit@MnFe₂O₄ was proven to be unrestricted in biology conditions.

Keywords: chitosan; magnetite; palladium magnetite; nitroarene reduction; allyl carbamate deprotection



Citation: Ebadi, M.; Asikin-Mijan, N.; Md. Jamil, M.S.; Iqbal, A.; Youisif, E.; Md Zain, A.R.; Aziz, T.H.T.; Rahimi Yusop, M. Palladium Nanoparticles on Chitosan-Coated Superparamagnetic Manganese Ferrite: A Biocompatible Heterogeneous Catalyst for Nitroarene Reduction and Allyl Carbamate Deprotection. *Polymers* **2023**, *15*, 232. <https://doi.org/10.3390/polym15010232>

Academic Editors: Constantinos Tsitsilianis, Jinglei Li and Coralia V. Garcia

Received: 7 October 2022

Revised: 27 October 2022

Accepted: 30 October 2022

Published: 1 January 2023



Copyright: © 2023 by the authors. Licensee MDPI, Basel, Switzerland. This article is an open access article distributed under the terms and conditions of the Creative Commons Attribution (CC BY) license (<https://creativecommons.org/licenses/by/4.0/>).

1. Introduction

In the field of catalysis, metallic nanocatalysts are known to possess higher catalytic activity due to their large surface-to-volume ratio [1–3]. To illustrate, gold nanoparticles NH₂-MIL-101(Fe) with easier biodegradability, superior catalytic activity, and less toxicity present promising strategies for industrial wastewater treatment [4]. Other researchers, R.T. Ledari et al., provided silver nanoparticles as a catalyst. These nanoparticles stabilized with volcanic pumice and chitosan and were acknowledged as higher-yield biomolecules in industrial applications [5]. However, nanosized-catalysts are usually involved in complicated isolation and recovery processes, as well as activity loss due to their aggregation [6–8]. Therefore, the constraints posed by nanosized-catalysts have become a challenge in the application of transition metals as a catalyst including palladium nanoparticles (Pd NPs). Palladium as a primary catalyst has been widely used in numerous applications. Several studies have been carried out to overcome the challenges involved in the use of Pd NPs as a catalyst by immobilizing the nanosized catalyst on insoluble metal supports such as silica [9,10], carbon [11,12], and polymeric materials [13–15]. For instance, I. Sargin et al. reported that the preparation of chitosan-carbon nanotube-supported palladium catalyst nanoparticles are efficient in reducing nitroarenes in industrial effluents [16]. Further

studies demonstrated that the catalytic potential of the Pd-graphene oxide nanocomposite was effective for the degradation of environmental contaminants [17]. Additionally, N-maleyl chitosan-supported palladium as an environmentally friendly catalyst exhibited high catalytic and economic performance [18].

In previous studies, magnetic materials were considered ideal supports for heterogeneous catalysts [19,20]. J. Rahimi et al. reported an organic–inorganic hybrid nanocomposite constructed of polyvinyl alcohol, iron oxide, and silver nanoparticles, which is a promising selection for an efficient catalytic system. They found that this nanocomposite has great catalytic performance, with high yields in short times for biological activity [21]. The magnetic-supported catalysts can be conveniently and easily recovered through the magnetic separation technique using an external magnetic field [22]. R.T. Ledari et al. reported a magnetic catalyst constructed of iron oxide and silver nanoparticles with an isothiazolone organic structure used for the conversion of nitrobenzene derivatives to their aniline forms. These nanoparticles are efficient catalysts with high magnetic properties and excellent reusability [23]. Moreover, F. H. Afruzi introduced a novel mesoporous nanocomposite that was magnetized by magnetite nanoparticles (APTES@SBA-15/Fe₃O₄), which exhibited excellent catalytic activity [24]. A wide range of magnetic catalysts are used for industrial purposes. For example, Sh. Bahrami et al. designed the magnetic biocompatible rod-like ZnS/CuFe₂O₄/agar organometallic hybrid catalyst with notable strengths [25]. Among the magnetic materials, nanoparticles of manganese ferrite (MnFe₂O₄), which is a type of spinel ferrite (MFe₂O₄, where M(II) is a d-block transition metal), have attracted much interest due to their high saturation magnetization (M_s) [26]. Moreover, MnFe₂O₄ usually exhibits superparamagnetic behaviour below the dimensions of 50 nm [27]. The superparamagnetic properties of MnFe₂O₄ allow it to be easily separated using a magnet and can be redispersed in the absence of an external magnetic field [28].

Coating magnetic nanoparticles with non-toxic materials prevents the degradation of their magnetic properties during catalytic reactions [29] and reduces the toxicity of toxic ferrite nanoparticles [30]. Among the various coating materials, biopolymers have gained much attention due to environmental issues [31]. Chitosan is one example of an eco-friendly biopolymer which exists abundantly in nature and can be obtained from organic waste at low production cost [32]. Besides that, chitosan is an ideal biopolymer for heterogeneous catalyst preparation because it only dissolves in acidic conditions but is insoluble in water and organic solvent [33]. Previous studies in the literature have reported that the amine functional group of chitosan can promote metal ion chelation [34]. This unique feature makes chitosan a suitable support for heterogeneous catalysts [35–37]. In addition to being biocompatible, biodegradable, and low toxicity, its good antibacterial and antitumor properties enable chitosan to be applied for biomedical and pharmaceutical purposes [38,39]. Biocompatible heterogeneous catalysts could play an important role in chemical engineering [40,41]. M. Kamalzare et al., explored and considered magnetic bio-nanocomposite synthesized with chitosan and tannic acid that obtained successful advantages for use as a heterogeneous nanocatalyst [42]. In another study, they prepared a bio-nanocatalyst based on magnetic nanoparticles and starch as a natural polymer that lists mild condition, low cost, and non-toxicity as some of the advantages [43].

One of the important reactions catalysed by palladium is nitroarene reduction such as reductions of 4-nitrophenol (4-NP) and 4-nitroaniline (4-NA) [44,45]. The 4-NP is a toxic organic pollutant and can be converted to a less toxic 4-aminophenol (4-AP) using a simple reductive reaction catalysed by Pd NPs in the presence of NaBH₄ as a reducing agent [46]. The 4-AP is a useful organic compound in pharmaceutical applications, such as the starting material for paracetamol synthesis [47]. The 4-NA is another nitroarene compound, which is classified as a type of hardly biodegradable organic pollutant commonly found in wastewater and associated with the dye synthesis industry [48]. It is toxic to aquatic organisms and harmful to human health after repeated exposure [49]. Therefore, the reduction of 4-NA to a more valuable and less toxic 4-phenylenediamine (4-PDA) is very important in many industries [50]. The 4-PDA produced from the reduction of the toxic

4-NA can be used as an ingredient in hair dyes [51], rubber antioxidants [52], aramid textile fibre intermediates, thermoplastics, and cast elastomers [53]. Besides nitroarene reduction, Pd can also play an important catalytic role in the allyl carbamate cleavage [54]. Due to the stability of allyl carbamate in acidic and basic conditions, it is widely used in the protection of the amine group that is crucial in certain organic synthesis reactions [55,56].

In this study, a novel chitosan-coated magnetic Pd NPs catalyst (Pd-Chit@MnFe₂O₄) was successfully designed for nitroarene reduction and allyl carbamate deprotection reactions. The magnetic material MnFe₂O₄ was coated with chitosan via the ionic gelation method to provide an ideal platform for metal ion immobilization on the support material. Subsequently, the immobilization of Pd NPs on the chitosan-coated MnFe₂O₄ was performed via the wet impregnation method. The physicochemical data and catalytic properties indicate that the catalyst has high potential for use in both chemical and biological systems.

2. Materials and Methods

2.1. Materials

Manganese (II) chloride tetrahydrate ($\geq 98\%$), 1-amino-2-propanol (MIPA, 93%), chitosan (75–80% deacetylated, medium molecular weight $\sim 190,000$ – $310,000$ Da), sodium tripolyphosphate (85%), palladium acetate (99.99%), 4-nitrophenol ($\geq 98\%$), sodium borohydride (98%), rhodamine 110, allyl chloroformate, pyridine, and thiophenol were obtained from Sigma-Aldrich. 4-Nitroaniline, iron(III) chloride hexahydrate, and hydrochloric acid (37%) were purchased from Merck. Nitric acid (65%) was acquired from Friedemann Schmidt. A 10% hydrazine hydrate solution was prepared in methanol solvent based on the method reported by Liew et al. [12]. Fresh HeLa cells and MTT (3-(4,5-dimethylthiazol-2-yl)2,5-diphenyl tetrazolium bromide) were obtained from the Advanced Medical and Dental Institute (IPPT), Universiti Sains Malaysia (USM). All organic solvents were of analytical grade and used without further purification. Deionized water (DIW) was used throughout the experiments.

2.2. Preparation of Pd-Chit@MnFe₂O₄

2.2.1. Preparation of MnFe₂O₄ Nanoparticles

MnFe₂O₄ nanoparticles were prepared using the coprecipitation method developed by Pereira et al. [57]. Solution A was prepared by mixing 10 mmol of MnCl₂·4H₂O with 5 mL of 0.1 M HCl (1:4 V/V) in a beaker. Solution B was prepared by dissolving 20 mmol of FeCl₃·6H₂O in 40 mL of DIW. Both solutions were heated to 50 °C and then quickly added to a beaker containing 200 mL of 3.0 M MIPA solution. The reaction mixture was heated to 100 °C and mechanically stirred for 2 h at 1000 rpm. The freshly prepared MnFe₂O₄ nanoparticles were magnetically isolated and dried under vacuum at room temperature overnight.

2.2.2. Preparation of Chitosan-Coated MnFe₂O₄

Chitosan-coated MnFe₂O₄ was prepared based on the method developed by Liew et al. [58]. The mass ratio of MnFe₂O₄ to chitosan was 1:1.25. The concentration of chitosan solution was 5 mg·mL⁻¹. The mass and volume ratio of chitosan to TPP used for ionic gelation was 5:1 and 5:2, respectively. The freshly prepared MnFe₂O₄ (100 mg) was dispersed in a beaker containing 25 mL of the acetic acid solution, followed by ultrasonication for 1 min at room temperature. Chitosan (125 mg) was added to the mixture and stirred at room temperature for 1 h at 1000 rpm. The TPP solution was prepared by dissolving 25 mg of TPP in 10 mL of DIW and then it was added dropwise to the MnFe₂O₄/chitosan mixture using a syringe pump at a rate of 1.0 mL·min⁻¹. The mixture was then stirred at 1000 rpm for 1 h at room temperature. The resulting product, Chit@MnFe₂O₄ was separated using a magnet, washed with water until pH = 7, and dried under vacuum at room temperature overnight.

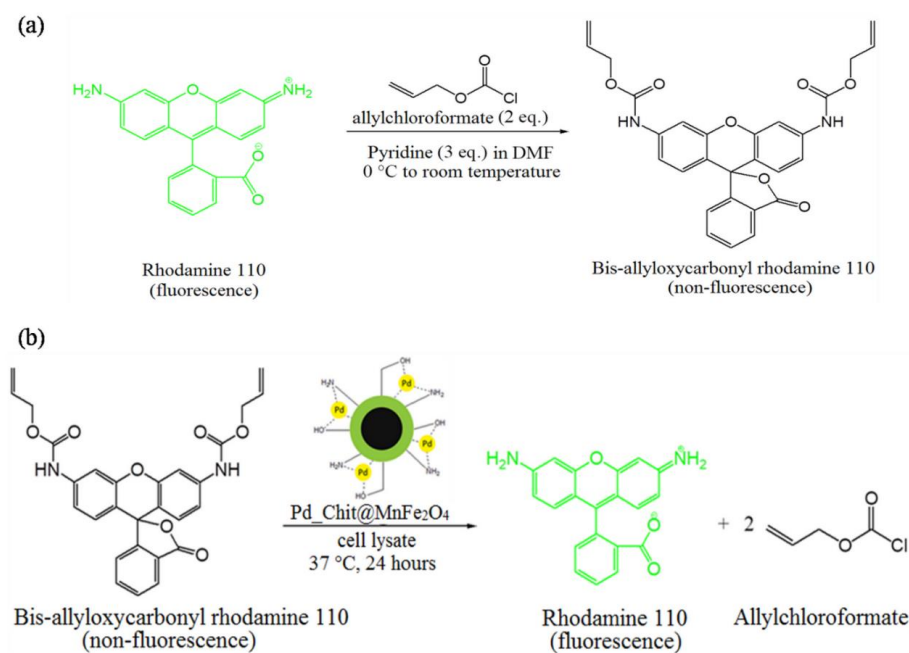
2.2.3. Preparation of Magnetic-Supported Pd Catalyst

Magnetic-supported Pd catalyst Pd-Chit@MnFe₂O₄ was prepared by adding 100 mg of Chit@MnFe₂O₄ in a beaker containing 5 mL of toluene and 0.05 mmol of Pd(OAc)₂

salt. The reaction mixture was stirred at 80 °C at 40 rpm for 10 min and then further stirred at room temperature for 2 h. Subsequently, the Pd²⁺ ion was reduced to Pd NPs by adding 10% hydrazine hydrate solution and stirred for 30 min at room temperature with a stirring speed of 40 rpm. The freshly prepared Pd-Chit@MnFe₂O₄ was then separated, washed with acetone, and dried under vacuum for 24 h. Superparamagnetic MnFe₂O₄ was first synthesized through the coprecipitation method by using MIPA as the alkaline agent. Subsequently, the superparamagnetic MnFe₂O₄ was coated with chitosan via the ionic gelation method using sodium tripolyphosphate (TPP) as a cross-linking agent. The coating approach resulted in tuned surface properties of MnFe₂O₄, which are ideal for use as a support for heterogeneous catalysts because chitosan has a high sorption capacity for metals and metal ions [59]. For Pd NPs immobilization, Pd(OAc)₂ was used as a Pd precursor to the introduction of free palladium(II) ions in toluene. The free palladium(II) ions were physically adsorbed on the surface of the Chit@MnFe₂O₄ via electrostatic interaction. The solid material was then treated with hydrazine hydrate to reduce the palladium(II) ions to metallic palladium nanoparticles (Pd NPs). The loading of Pd on Pd-Chit@MnFe₂O₄ was further investigated by ICP-MS.

2.2.4. Preparation of Rhodamine 110

Bis-allyloxycarbonyl-protected rhodamine 110 was produced based on the method published by Streu and Meggers [40]. Rhodamine 110 (0.5 mmol) was dissolved in 1.2 mL of dry *N,N'*-dimethylformamide (DMF). The reaction mixture was cooled down to 0 °C under an inert atmosphere. A mixture of allyl chloroformate (1.0 mmol) and pyridine (1.5 mmol) in DMF (0.5 mL) was prepared and then added dropwise to the previous solution containing rhodamine 110. The reaction mixture was warmed to room temperature and stirred for 24 h. The product was extracted using ethyl acetate and concentrated under a vacuum. Column chromatography technique was performed by using hexane: ethyl acetate (2:1) to obtain the pure product. The preparation of non-fluorescence bis-allyloxycarbonyl-protected rhodamine 110 from a fluorescence compound rhodamine 110 by using allyl chloroformate is shown in Scheme 1.



Scheme 1. (a) Synthesized of non-fluorescence bis-allyloxycarbonyl protected rhodamine 110 and (b) Palladium-induced allyl carbamate cleavage by Pd-Chit@MnFe₂O₄ in HeLa cell lysate to produce fluorescence rhodamine 110. The product of the reaction was fluorescence rhodamine 110. This reaction was important to confirm the catalytic performance of Pd-Chit@MnFe₂O₄ was not inhibited by components present in cells.

2.3. Catalyst Characterization

2.3.1. Structural Analysis

The structure changes on the synthesized sample were investigated using X-ray diffraction (XRD, Bruker D8-Advanced (Bruker AXS, Bremen, Germany)). The instrument employed Cu-K α radiation ($\lambda = 0.15406$ nm) at 30 kV and 15 mA, and scans were conducted over the 2θ range of $20^\circ \leq 2\theta \leq 80^\circ$ with a scanning rate of 2° min^{-1} . The patterns were matched to the Joint Committee of Powder Diffraction Standard (JCPDS)'s database. The average crystallite size of Pd and MnFe₂O₄ was calculated by using the Debye–Scherrer formula [60]. The elemental composition and chemical state of the catalyst were determined using X-ray photoelectron spectrometry (XPS) analysis (Kratos Axis Ultra DLD X-ray photoelectron spectrometer). The catalyst sample was prepared in a pellet formed for XPS analysis. The determination of the functional group present on the prepared catalyst was investigated using Fourier transform infrared (FTIR) spectra using Agilent Technologies Cary 630 FTIR spectrometer in the range of 650–4000 cm⁻¹. Furthermore, the morphology and particle size of the catalyst was examined by transmission electron microscopy (TEM) using Philips CM 12 transmission electron microscope at 100 kV and field emission scanning electron microscopy (FESEM) using SUPRA 55VP Zeiss scanning electron microscope.

2.3.2. Elemental Analysis

The elemental composition of the Pd immobilized on the surface of Chit@MnFe₂O₄ was determined by inductively coupled plasma mass spectrometry (ICP-MS) using a Perkin Elmer ELAN 9000 ICP mass spectrometer (USA). The loading of Pd immobilized on the surface of Chit@MnFe₂O₄ was determined by dissolving 1.0 mg of Pd-Chit@MnFe₂O₄ in 3 mL aqua regia. The solution was then topped-up with water to a total volume of 25 mL. The amount of Pd in the solution was determined by ICP-MS.

2.3.3. Magnetic Properties

The magnetic properties of the sample were analysed using vibrating sample magnetometry (VSM) (LakeShore 7404 series) vibration sample magnetometer. To distinguish the metal-oxygen species in the catalyst precursors, UV-Vis measurements were performed using a Shimadzu UV-2450 UV-Vis spectrophotometer over a wavelength range of 200–800 nm.

2.3.4. Catalytic Activity

Catalytic Reduction of Nitroarene Compounds and Reusability

The catalytic activity of Pd-Chit@MnFe₂O₄ was investigated in nitroarene (4-NP and 4-NA) reduction using NaBH₄ as a reducing agent. In a typical reaction, 0.15 mmol of NaBH₄ was added to 3 mL of 0.05 mM 4-NP solution, resulting in a yellow-green solution of 4-nitrophenolate. The Pd-Chit@MnFe₂O₄ was then added to the solution mixture and the conversion of 4-NP to 4-AP took place immediately. The reduction reaction was monitored using a UV-Vis spectrometer. The optimization of 4-NP reduction was performed with the same procedures by using different masses (0.5 and 1.0 mg) of Pd-Chit@MnFe₂O₄. The reduction of 4-NA to 4-PDA was also carried out with the same experimental conditions by using 0.5 mg of Pd-Chit@MnFe₂O₄ as the catalyst. Control experiments were carried out for both 4-NP and 4-NA reduction respectively by replacing the catalyst with MnFe₂O₄, Chit@MnFe₂O₄, and without catalyst. The rate of reaction was calculated from the pseudo-first-order kinetic model:

$$\ln(A/A_0) = -kt \quad (1)$$

where A is the concentration of nitroarene compound at t time, A_0 is the initial concentration of 4-NP or 4-NA and k is the rate of the reaction [28]. For a more accurate comparison, the turnover frequency (TOF) value was calculated according to the equation:

$$\text{TOF} = n_0 / (n_{pd} \times \text{reaction time}) \quad (2)$$

where n_0 is the initial amount of 4-NP or 4-NA and n_{Pd} is the number of Pd active sites on the catalyst used. The reusability of Pd-Chit@MnFe₂O₄ was tested using 20 times scale-up nitroarene reduction in a 50 mL round bottom flask with the same reaction conditions. The catalyst was isolated using a magnet, washed with water, and used in the next cycle of nitroarene reduction. The mass of the isolated catalyst was weighed after all 8 cycles of nitroarene reduction were completed.

Deprotection of Bis-allyloxycarbonyl Rhodamine 110 with and without Thiophenol

Deprotection of bis-allyloxycarbonyl rhodamine 110 was performed according to the method developed by Yusop et al. [41]. Deprotection of bis-allyloxycarbonyl rhodamine 110 was carried out in two conditions, with thiophenol, and without thiophenol. For the condition with thiophenol, 1.5 μ mol of bis-allyloxycarbonyl-protected rhodamine 110 in dimethyl sulfoxide (DMSO) (75 μ L, 20 mM) was added to 2.72 mL of the cell lysate solution, followed by the addition of 150 μ L of a 100 mM thiophenol solution in DMSO. Then, 60 μ L of Pd-Chit@MnFe₂O₄ in DIW (10 mM, Pd loading of 0.6 μ mol) was added to the mixture. The final reaction mixture (3 mL) was shaken at 300 rpm at 37 °C for 24 h. The reaction was monitored by thin-layer chromatography (TLC) and observed under UV light. For the reaction without thiophenol, 1.5 μ mol of bis-allyloxycarbonyl-protected rhodamine 110 in DMSO (75 μ L, 20 mM) was added to 2.87 mL of cell lysate solution, followed by the same amount of Pd-Chit@MnFe₂O₄. A negative control experiment also was carried out without adding Pd-Chit@MnFe₂O₄ and thiophenol for comparison. Negative control was performed by adding 2.93 mL of the cell lysate solution to 1.5 μ mol of bis-allyloxycarbonyl-protected rhodamine 110 in DMSO (75 μ L, 20 mM).

Stability and Cytotoxicity of Pd-Chit@MnFe₂O₄

The stability of Pd-Chit@MnFe₂O₄ was investigated by robustness test. Approximately 1.0 mg of Pd-Chit@MnFe₂O₄ was dispersed in 10 mL of DIW and heated to 80 °C for 20 min with a stirring speed of 40 rpm. The Pd-Chit@MnFe₂O₄ was filtered off and the filtrate was examined by ICP-MS. The robustness test for Pd on manganese ferrite without coating was carried out using the same procedure as Pd-Chit@MnFe₂O₄. A cytotoxicity test was carried out on the HeLa cell by using an MTT assay with two concentrations of Pd-Chit@MnFe₂O₄, which were 1.25×10^{-1} mg·mL⁻¹ and 2.5×10^{-1} mg·mL⁻¹ of Pd-Chit@MnFe₂O₄ in DIW. A cell density of 5000 cells/well was plated in a 96-well plate and allowed to grow for 24 h. Then, the Pd-Chit@MnFe₂O₄ was added to the well-incubated HeLa cell and monitored with a fluorescence microscope. After 24 h, the cytotoxicity test result was compared with the untreated cell. The cytotoxicity test was performed in triplicate for both concentrations of Pd-Chit@MnFe₂O₄.

3. Results and Discussion

3.1. Structural Analysis

The XRD diffractogram of Chit@MnFe₂O₄ and Pd-Chit@MnFe₂O₄ are shown in Figure 1a. The result showed there are ten diffraction peaks related to the MnFe₂O₄ with spinel cubic crystal can be observed at $2\theta = 18.5^\circ, 30.0^\circ, 35.5^\circ, 37.0^\circ, 42.5^\circ, 53.0^\circ, 56.5^\circ, 62.0^\circ, 70.0^\circ,$ and 73.5° . These 2θ correspond to the (111), (220), (311), (222), (400), (422), (511), (440), (620), and (533) planes of the MnFe₂O₄ crystal's unit cell (JCPDS 01-073-3820), respectively [61,62]. From the XRD diffractogram of Pd-Chit@MnFe₂O₄, three weak diffraction peaks were observed at $2\theta = 40.1^\circ, 46.6^\circ,$ and 68.3° , which were assigned to the (111), (200), and (220) planes of Pd(0), respectively, with a face-centred cubic lattice structure (JCPDS 00-046-1043) [63]. The weak intensity of the diffraction peaks is due to the low Pd content on the catalyst surface. However, the intensity of diffraction peaks related to MnFe₂O₄ reduced due to chitosan coating and immobilization of Pd NPs [64]. The mean crystallite size of MnFe₂O₄ was calculated using the Scherrer equation was determined to be 11.9 nm whereas the mean crystallite size of Pd was around 3.4 nm. Noteworthy to mention, the diffraction peaks related to chitosan were not observed in the XRD diffractogram of

Chit@MnFe₂O₄ and Pd-Chit@MnFe₂O₄ due to the amorphous nature of chitosan or due to the formation of a thin chitosan layer [65]. The presence of diffraction peaks related to MnFe₂O₄ in the diffractogram of Chit@MnFe₂O₄ and Pd-Chit@MnFe₂O₄ indicates that its crystallinity is preserved even in the presence of chitosan and Pd.

The XPS spectrum of Pd 3d is given in Figure 1b–c. The deconvolution of the spectrum resulted in two peaks centred at BE = 334.8 eV and BE = 340.8 eV. The first peak is attributed to the Pd 3d_{5/2} whereas the latter is attributed to the Pd 3d_{3/2}, which can be ascribed to metallic Pd. The presence of these peaks confirmed that Pd²⁺ was mainly reduced to metallic Pd. The presence of these peaks confirmed that Pd²⁺ was mainly reduced to metallic Pd. The XPS result is consistent with the previously reported reports [66]. The minor peaks located at 338.2 eV (Pd 3d_{5/2}) and 343.4 eV (Pd 3d_{3/2}) correspond to Pd(II) species, which have indicated the interaction of metallic Pd with amine groups in chitosan [67,68].

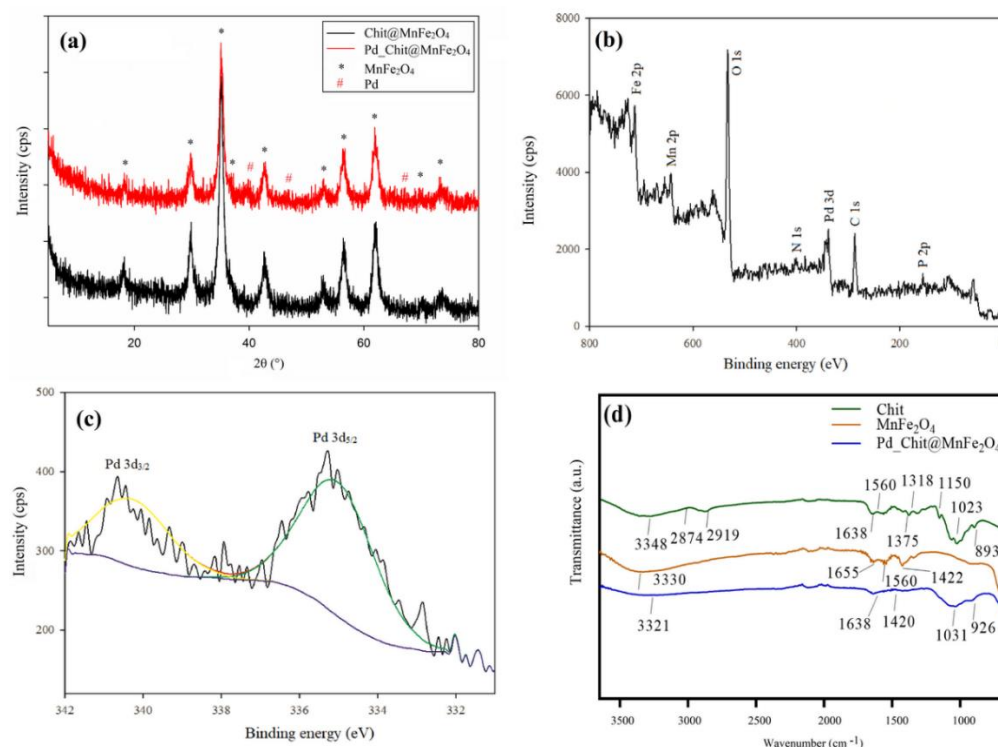


Figure 1. (a) XRD patterns, (b) wide scan XPS spectrum, (c) Pd 3d high resolution XPS spectrum and (d) FTIR spectrum of Pd-Chit@MnFe₂O₄.

Figure 1d shows the FTIR spectrum of chitosan, MnFe₂O₄, and Pd-Chit@MnFe₂O₄. In the FTIR spectrum of chitosan, the absorption band showed at 3348 cm⁻¹ (–O–H) [69], 2874 cm⁻¹ and 2919 cm⁻¹ (–CH₂ and –CH₃) [70], 1638 cm⁻¹, 1560 cm⁻¹, and 1318 cm⁻¹ (–C=O, stretching of amide I, –N–H bending of amide II, and –C–N stretching of amide III) [71], 1375 cm⁻¹ (–C–H) [72], 893 cm⁻¹ and 1150 cm⁻¹ (C–O–C stretching of glycosidic linkages) [73], 1060 cm⁻¹ and 1023 cm⁻¹ (–C–O stretching vibration of a secondary alcohol and primary alcohol), respectively [74]. A similar trend was observed on Pd-Chit@MnFe₂O₄, yet Pd-Chit@MnFe₂O₄ showed shifting of the stretching vibrations of chitosan's (–C–O–C) from 1023 to 1031 cm⁻¹. The shifting indicates that the bond strengths of C–O–C in glycosidic bonds increased due to environmental differences after the ionic gelation process [75]. Noted, it also implied that manganese ferrite was successfully coated with chitosan via cross-linked TPP. The case of MnFe₂O₃ showed the elimination of absorption peaks belonging to –CH₂, –CH₃, and C–O–C. The morphology and particle size distributions of Chit@MnFe₂O₄ and of Pd-Chit@MnFe₂O₄ were characterized by SEM and TEM analyses, respectively. From Figure 2a,c, it can be observed that the MnFe₂O₄ particles were mostly spherical-shaped with various sizes. The surface morphology of the catalyst

was spherically shaped as well (Figure 2e). The average diameter of Pd-Chit@MnFe₂O₄ determined from the TEM image was about 11 ± 5 nm (Figure 2b) whereas the average diameter of Pd-Chit@MnFe₂O₄ determined from the SEM image was 10 ± 2 nm (Figure 2f). Figure 2c is the TEM micrograph of Chit@MnFe₂O₄ showing the average particle size from the corresponding diameter distribution, which is in the range of 6 nm (Figure 2d). Thus, the reported higher size in Pd-Chit@MnFe₂O₄ is due to the capping of Pd nanoparticles. The catalytic activity of the Pd catalyst is probably due to the following effects: A high absorption capacity was provided by the morphology of Pd nanocomposite which in turn, decreased the induction time. Additionally, the catalytic activity was improved due to the strong synergistic effects of its constituents. (–NO₂) group can be reduced to an amine and aniline by the Pd-Chit@MnFe₂O₄ nanocomposite. Without Pd as catalytic hydrogenation, the catalytic reduction reaction cannot proceed. As the catalyst was added into the system, ions were adsorbed by Pd, due to strong adsorption capacity and reduction reaction removed oxygen and added hydrogen. Then the active species reduced –NO₂ into –NH₂, which indicated the catalyst's critical role in this reduction. In Figure 2h, EDS analysis indicates that Pd-Chit@MnFe₂O₄ was mainly composed of C, O, Fe, and Mn, P, and Pd. The P originated from the CS cross-linked with the TPP ion by ionic gelation [58]. The EDS and mapping micrograph proved that the immobilized Pd NPs were well-dispersed on the Chit@MnFe₂O₄ support (Figure 2g).

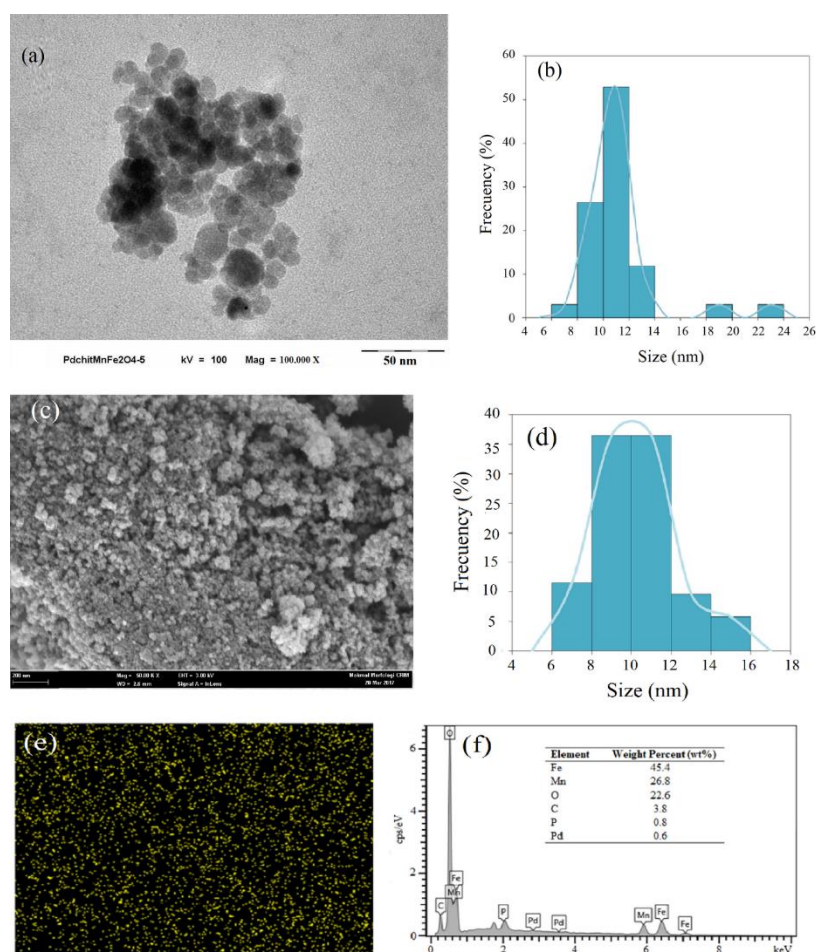


Figure 2. (a) TEM micrograph of Pd-Chit@MnFe₂O₄, (b) the size distribution histogram from TEM micrograph, (c) TEM micrograph of Pd, (d) the size distribution histogram from TEM micrograph, (e) SEM micrograph of Pd-Chit@MnFe₂O₄, (f) the size distribution histogram from SEM micrograph, (g) mapping micrograph for Pd NPs, and (h) EDS data of Pd-Chit@MnFe₂O₄.

3.2. Elemental Analysis

The total concentration of Pd, Mn, and Fe in Pd-Chit@MnFe₂O₄ detected by ICP-MS analysis is given in Table 1. The loading of Pd on Pd-Chit@MnFe₂O₄ was determined to be 0.21 mmol·g⁻¹. The atomic ratio of Fe: Mn was determined to be 2:1, which agrees with the molecular formula of MnFe₂O₄. The robustness test indicates that higher Pd leached out from the MnFe₂O₄ without chitosan coating. The concentration of Pd detected was 26.6 ppb or 0.03 wt%. The Pd concentration was reduced to 10.8 ppb or 0.01 wt% when the MnFe₂O₄ was coated with chitosan. The observation indicates that the Pd-Chit@MnFe₂O₄ is safe to be used in the pharmaceutical industry as the leaching level of Pd from the catalyst was lower than the maximum acceptable concentration limits [76,77].

Table 1. ICP-MS results for Pd-Chit@MnFe₂O₄. *1.0 mg Pd-Chit@MnFe₂O₄ was dissolved in 3 mL aqua regia and top-up with water to a total volume of 25 mL.

Analyte	Mean Concentration (ppb)	Metal Loading (mmol/g)	Simplest Ratio
Palladium (Pd)	912.75	0.21	-
Manganese (Mn)	7286.01	3.32	1
Iron (Fe)	13,523.70	6.05	1.8

3.3. Magnetic Properties

The magnetic properties of Pd-Chit@MnFe₂O₄ were observed using VSM at room temperature and the magnetization curves are shown in Figure 3 and Table 2. The MnFe₂O₄, Chit@MnFe₂O₄, and Pd-Chit@MnFe₂O₄ retained high saturation magnetization (M_s) with low coercivity (H_c) and negligible remanent magnetization (M_r). The low squareness ratio (M_r/M_s) of MnFe₂O₄ (0.03), Chit@MnFe₂O₄ (0.03), and Pd-Chit@MnFe₂O₄ (0.05) confirmed their superparamagnetic behaviour [78]. Of note, the M_s value of MnFe₂O₄ was slightly higher than that of Chit@MnFe₂O₄ because of the chitosan coating around MnFe₂O₄ [79], whereas the decrease in the M_s value of Pd-Chit@MnFe₂O₄ indicated that Pd was successfully immobilized on Chit@MnFe₂O₄ [80]. The coating of chitosan and immobilization of Pd form a magnetically disordered layer around MnFe₂O₄, which results in a decrease in the total amount of magnetic phase of the support material and catalyst. The superparamagnetic properties of Pd-Chit@MnFe₂O₄ allowed the catalyst to be easily separated and recycled by applying an external magnetic field; it was redispersed when the external magnetic field was removed.

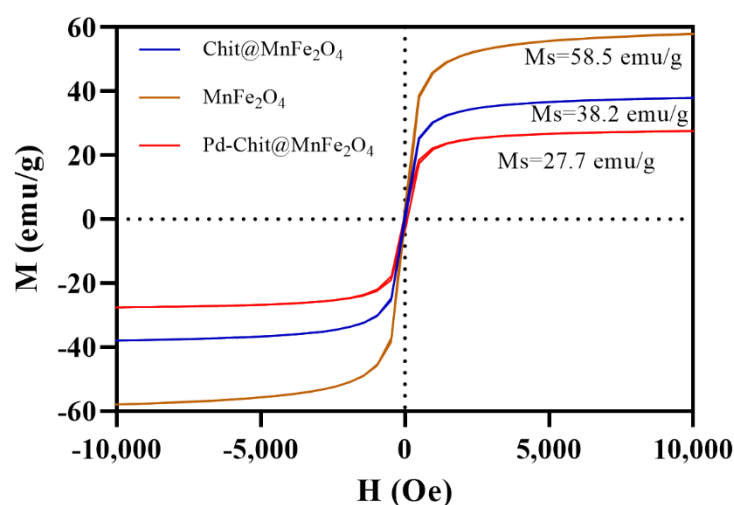


Figure 3. Magnetization curves of MnFe₂O₄, Chit@MnFe₂O₄, and Pd-Chit@MnFe₂O₄.

Table 2. Magnetic properties of MnFe_2O_4 , $\text{Chit@MnFe}_2\text{O}_4$, and $\text{Pd-Chit@MnFe}_2\text{O}_4$.

Nanomaterial	Magnetic Characterization			
	M_s (emu/g)	H_c (O_e)	M_r (emu/g)	M_r/M_s
MnFe_2O_4	58.4	22.8	2.0	0.03
$\text{Chit@MnFe}_2\text{O}_4$	38.2	22.5	1.2	0.03
$\text{Pd-Chit@MnFe}_2\text{O}_4$	27.7	31.4	1.3	0.05

3.4. Catalytic Activity

3.4.1. Catalytic Reduction of Nitroarenes and Reusability

The catalytic performance of $\text{Pd-Chit@MnFe}_2\text{O}_4$ was investigated in the reduction of 4-NP and 4-NA using NaBH_4 as a reducing agent. Due to the excess NaBH_4 , the reaction rate depends only on the concentration of the nitroarene compound. Hence, a pseudo-first-order kinetic plot was used to study the rate constant of the nitroarene reduction (Figure 4b,d). The 4-NP reduction profile is shown in Figure 4a. The absorption band at 400 nm belongs to the 4-nitrophenolate ion, which was formed when NaBH_4 was added to the 4-NP solution [81]. The absorption band continuously decreased in the presence of the catalyst. The reduction of the 4-nitrophenolate ion is accompanied by the formation of a new absorption band around 300 nm, which indicates the formation of 4-AP [82].

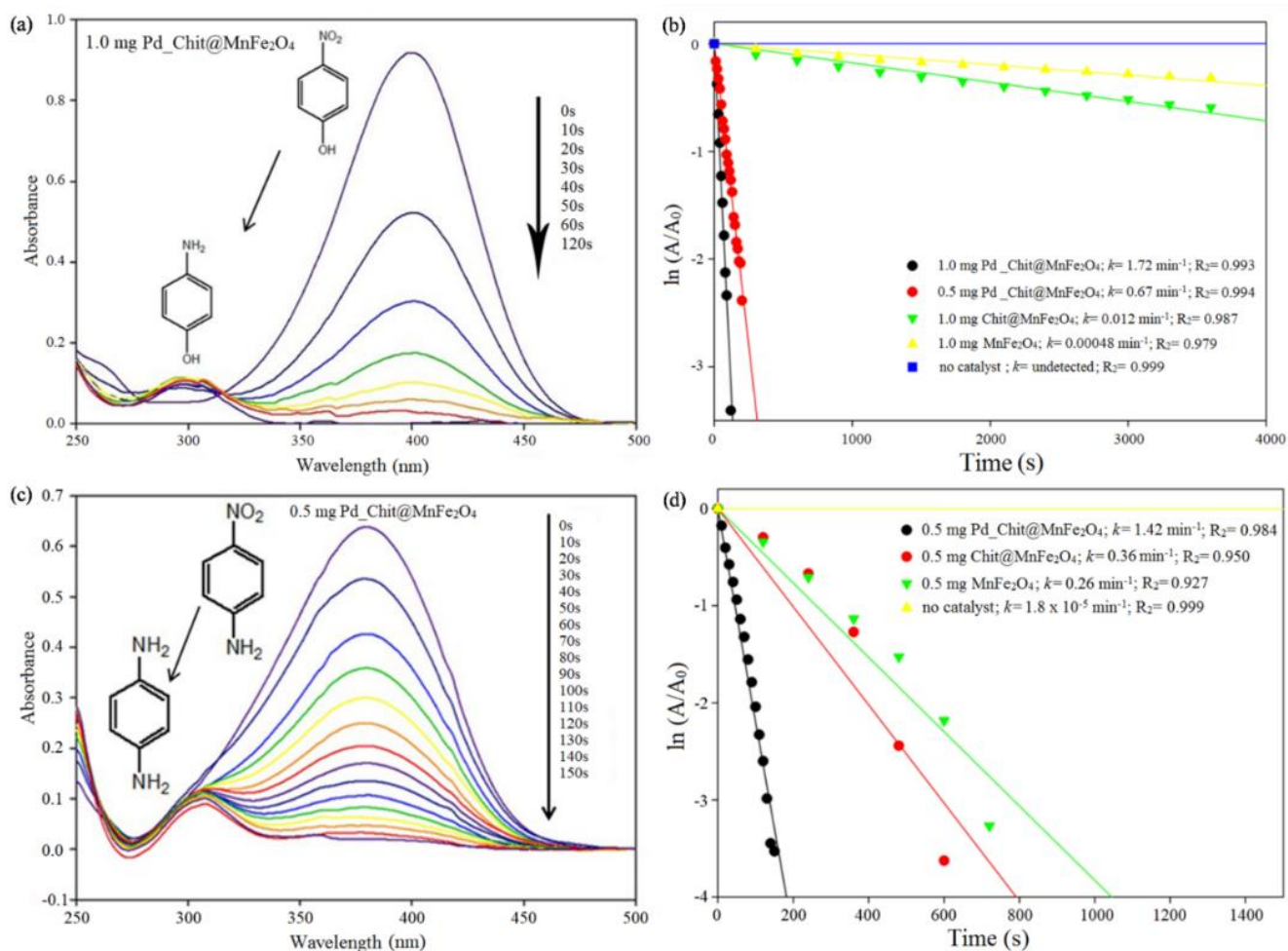


Figure 4. 4-NP reduction's (a) UV-Vis spectra with 1.0 mg $\text{Pd-Chit@MnFe}_2\text{O}_4$ and (b) pseudo-first-order kinetic plot (c) UV-Vis spectra with 0.5 mg $\text{Pd-Chit@MnFe}_2\text{O}_4$ and (d) pseudo-first-order kinetic plot.

The effect of catalyst type and the effect of Pd-Chit@MnFe₂O₄ mass on the 4-NP reduction reaction was also investigated. The pseudo-first-order plot of the 4-NP reduction is shown in Figure 4b, whereas the *k* and TOF values are summarized in Table 3. The catalytic reduction of 4-NP was low when Chit@MnFe₂O₄ and MnFe₂O₄ were applied as catalysts. Upon the addition of 0.5 mg of Pd-Chit@MnFe₂O₄, the reduction reaction of 4-NP requires 200 s to complete with a rate of reaction of 0.67 min⁻¹ and a TOF of 285.7 min⁻¹. The increase in the rate of catalytic reduction of 4-NP confirmed that Pd plays an important role in the reduction of 4-NP. When the mass of Pd-Chit@MnFe₂O₄ increased to 1.0 mg, the reaction time was reduced to 120 s. The *k* and TOF values for 1.0 mg of Pd-Chit@MnFe₂O₄ were 1.72 min⁻¹ and 357.1 min⁻¹, respectively.

Table 3. The chemical equation and comparison of catalytic performance of Pd-Chit@MnFe₂O₄ for the 4-NP and 4-NA reduction in various experimental conditions.

The chemical equation of nitroarene reduction:

X = OH or NH₂

O=[N+]([O-])c1ccc(X)cc1
 $\xrightarrow[\text{NaBH}_4]{\text{Pd_Chit@MnFe}_2\text{O}_4}$
Nc1ccc(X)cc1

Nitroarene Aniline

Condition	Time (s)	<i>k</i> (min ⁻¹)	TOF (min ⁻¹)
(a) 4-NP reduction *:			
1.0 mg Pd-Chit@MnFe ₂ O ₄	120	1.72	357.1
0.5 mg Pd-Chit@MnFe ₂ O ₄	200	0.67	285.7
1.0 mg Chit@MnFe ₂ O ₄	3600	0.012	-
1.0 mg MnFe ₂ O ₄	3600	0.0048	-
Without catalyst	3 days	-	-
(b) 4-NA reduction *:			
0.5 mg Pd-Chit@MnFe ₂ O ₄	150	1.42	571.4
0.5 mg Chit@MnFe ₂ O ₄	600	0.36	-
0.5 mg MnFe ₂ O ₄	720	0.26	-
Without catalyst	1 day	0.000018	-

* (a) 4-NP and (b) 4-NA stands for 4-nitrophenol and 4-nitroaniline, respectively.

The catalytic activity of Pd-Chit@MnFe₂O₄ was further evaluated in the reduction of 4-NA. From Figure 4c, the intensity of an absorption band around 380 nm associated with 4-NA decreased as the reaction continued [83]. The reduction in the absorption intensity of 4-NA is accompanied by the rise in an absorption band associated with 4-PDA around 305 nm [40]. For the control experiment, the pseudo-first-order plots of 4-NA reduction are illustrated in Figure 4d, whereas the *k* and TOF values are shown in Table 3. In the control experiments, the reaction rate was slow when the experiment was conducted with 0.5 mg of Chit@MnFe₂O₄ and MnFe₂O₄. The conversion of 4-NA to 4-PDA was negligible without a catalyst. Noteworthy, when 0.5 mg Pd-Chit@MnFe₂O₄ was added, the reduction of 4-NA was catalysed at a higher reaction rate of 1.42 min⁻¹ and TOF value of 571.4 min⁻¹. The complete reaction time was reduced to 2.5 min. Overall, the results showed that Pd-Chit@MnFe₂O₄ has superior catalytic activity in a reduction reaction of 4-NP and 4-NA.

The pseudo-first-order kinetic plot of 8 consecutive cycles of 4-NP and 4-NA reduction reactions is displayed in Figures 5a and 5b, respectively. Results show that the conversion of 4-NP and 4-NA was ~100% for 8 consecutive cycles (as shown in Figure 5c), which indicated that Pd-Chit@MnFe₂O₄ was stable and can be reused up to 8 consecutive cycles.

The minimum loss of catalyst nanoparticles during the recycling process may lead to a slight increase in reaction time upon cycles for both 4-NP and 4-NA reduction.

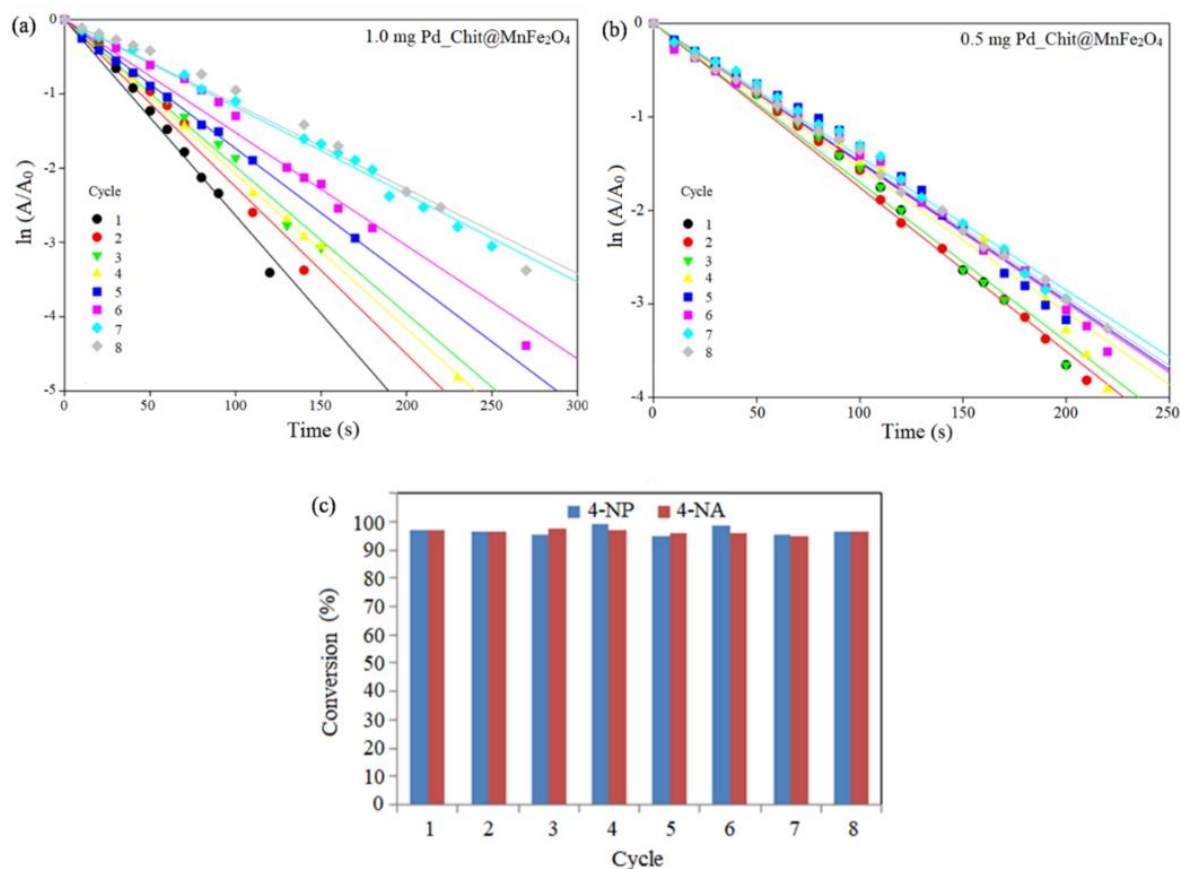


Figure 5. Reusability of Pd-Chit@MnFe₂O₄ in (a) 4-NP and (b) 4-NA reductions and (c) conversion of 4-NP and 4-NA reduction.

A plausible mechanism was proposed for Pd-Chit@MnFe₂O₄ catalysed nitroarenes reduction based on the Langmuir–Hinshelwood model and Haber mechanism [84,85]. The proposed mechanism is shown in Figure 6. First, both reactants adsorbed on the surface-active site of Pd-Chit@MnFe₂O₄ based on the Langmuir–Hinshelwood model. After the adsorption process, electron transfer occurred between the nitroarene compound and hydride ion, followed by the dehydration process to yield the nitroso compound. The nitroso compound undergoes further reduction to form hydroxylamine compound in a very fast step. Next, the hydroxylamine compound was finally converted to an amine compound via a series of electron transfers followed by the dehydration process. At the end of the catalytic cycle, the amine compound as product desorbed from the surface of Pd-Chit@MnFe₂O₄, and a new catalytic cycle will begin.

3.4.2. Palladium-Induced Allyl Carbamate Deprotection

From Figure 7 (entry 1), the control experiment showed that no product was formed (no fluorescence detected) in the absence of Pd-Chit@MnFe₂O₄, whereas the deprotection of bis-allyloxycarbonyl rhodamine 110 was successfully performed in the presence of Pd-Chit@MnFe₂O₄ with and without thiophenol (Figure 7: entry 3). Notably, our newly designed catalyst Pd-Chit@MnFe₂O₄ successfully catalysed allyl carbamate cleavage without thiophenol as a scavenger (Figure 7: entry 2). High levels of thiophenol have proven to be toxic to living organisms and the environment; therefore, this approach without thiophenol is highly beneficial [86]. The characterization of the reaction products formed after the reaction was determined by the purification and analysis of the cell lysate, which quanti-

tatively confirmed the chemical identities via liquid chromatography–mass spectrometry (LC-MS) and high-performance liquid chromatography (HPLC). The reaction mixture was centrifuged for 5 min at 13,000 rpm. The supernatant was collected and passed through a DSC-18LT column which had been prewashed with water. The column was washed with water to remove salts and proteins from the cell lysate, and acetonitrile was used to elute the desired product from the column. The residue was dissolved in methanol and analysed by LC-MS in a positive ionization mode. LC-MS suggested the presence of rhodamine 110 with the m/z found at 331.0. In addition, HPLC analysis of the cell lysate showed retention times with a sample standard of around 3.2 min.

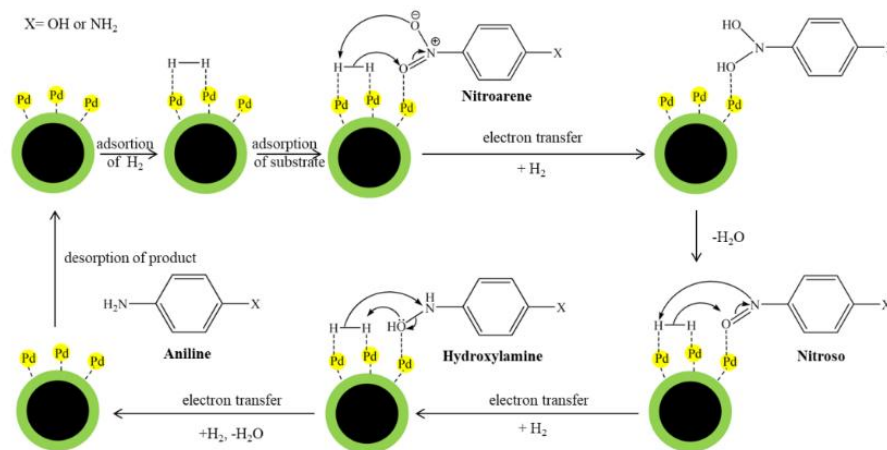


Figure 6. The proposed mechanism for Pd-Chit@MnFe₂O₄ catalyzed nitroarenes reduction, which involved adsorption of reactants, transfer of electrons, and adsorption of the product occurred at the surface of the catalyst.

Entry	1	2	3
Bis-allyloxycarbonyl rhodamine 110	+	+	+
Pd_Chit@MnFe ₂ O ₄	-	+	+
Thiophenol	-	-	+

Figure 7. Deprotection of bis-allyloxycarbonyl rhodamine 110 in 3 different conditions. Reaction conditions: Entry 1: negative control using bis-allyloxycarbonyl rhodamine 110 in DMSO (75 μ L, 20 mM) and cell lysate solution (2.93 mL); Entry 2: bis-allyloxycarbonyl rhodamine 110 in DMSO (75 μ L, 20 mM), cell lysate solution (2.87 mL) and Pd-Chit@MnFe₂O₄ in water (60 μ L, 10 mM); Entry 3: bis-allyloxycarbonyl rhodamine 110 in DMSO (75 μ L, 20 mM), cell lysate solution (2.72 mL), Pd-Chit@MnFe₂O₄ in water (60 μ L, 10 mM), and thiophenol in DMSO (150 μ L, 100 mM). All reactions were shaken at 300 rpm for 24 h at 37 $^{\circ}$ C.

3.5. Cytotoxic Assay

A HeLa cell was chosen to investigate the cytotoxicity of Pd-Chit@MnFe₂O₄ because of the cell's ability to grow rapidly and easily [87]. Figure 8 depicts the cytotoxic evaluation of Pd-Chit@MnFe₂O₄. As can be seen, Pd-Chit@MnFe₂O₄ caused low necrosis of HeLa cells and high cell viability (>89%) was observed after 24 h. The viability of HeLa cells treated with Pd-Chit@MnFe₂O₄ at two concentrations was found to have no substantial cytotoxicity. Previous literature has reported on low cytotoxicity heterogeneous Pd catalyst catalysing Suzuki–Miyaura cross-coupling and allyl carbamate cleavage in vivo [41]. Due to the low cytotoxicity of Pd-Chit@MnFe₂O₄, the Pd-Chit@MnFe₂O₄ catalyst is suggested as a potential candidate for catalysis in living systems.

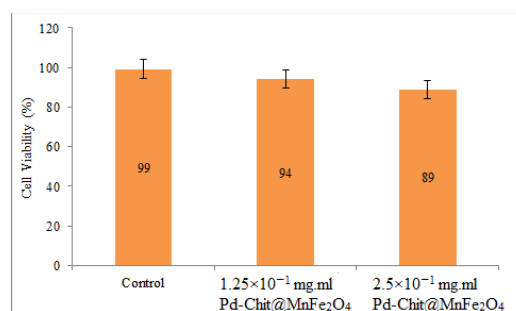


Figure 8. Cytotoxicity of Pd-Chit@MnFe₂O₄ on HeLa cells at 24 h.

3.6. BET Analysis

The surface area of the pure Pd and Pd-Chit@MnFe₂O₄ samples was estimated by Brunauer–Emmett–Teller surface area analysis (BET) (Figures 9a and 9b, respectively). According to the results, the surface area of 25.614 and 2.292 m²·g⁻¹ were found for palladium nanoparticles. The higher BET specific surface area of the Pd-Chit@MnFe₂O₄ nanocomposite compared with pure Pd can be ascribed to the introduction of Chit@MnFe₂O₄ particles in the composite and is beneficial to improve the catalytic performance.

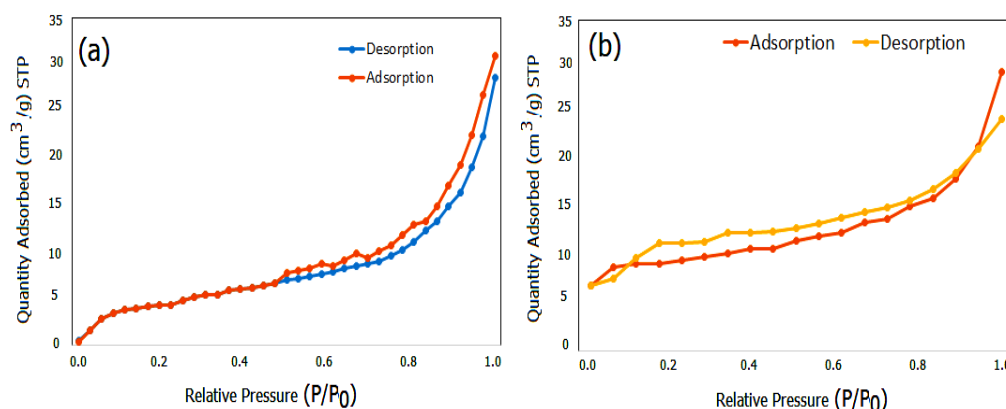


Figure 9. BET surface area analysis of (a) palladium nanoparticles, (b) Pd-Chit@MnFe₂O₄.

4. Conclusions

Chit@MnFe₂O₄ was successfully prepared and used as supporting material for heterogeneous Pd NP catalysts. This newly prepared Pd-Chit@MnFe₂O₄ catalyst demonstrated high catalytic activities in nitroarene reduction as well as excellent catalytic performance in the deprotection of allyl carbamate under biological conditions. Moreover, Pd-Chit@MnFe₂O₄ was stable for reuse and could be recycled with negligible loss of catalytic activity. The recovery process of Pd-Chit@MnFe₂O₄ was easy and convenient due to its superparamagnetic properties. Furthermore, this magnetically active chitosan-coated Pd catalyst is biocompatible and eco-friendly because it exhibited low cytotoxicity and

minimal leaching problems. Thus, it could be suitable for a variety of chemical applications. The biocompatible Pd-Chit@MnFe₂O₄ is of interest for future applications, predominantly in biomedical and clinical research.

Author Contributions: M.E.; writing—original draft preparation and formal analysis, N.A.-M.; writing—review and editing and formal analysis, M.S.M.J.; writing—review and editing and formal analysis, A.I.; writing—review and editing, E.Y.; writing—review and editing, A.R.M.Z.; funding acquisition and visualization, T.H.T.A.; funding acquisition and visualization, M.R.Y.; Conceptualization and methodology and project administration and funding acquisition. All authors have read and agreed to the published version of the manuscript.

Funding: This research and the APC was funded by Research Grant Scheme FRGS/1/2022/STG05/UKM/02/4 and this research was funded by UKM Research University Grant, grant numbers GUP-2019-045.

Institutional Review Board Statement: Not applicable.

Informed Consent Statement: Not applicable.

Data Availability Statement: Not applicable.

Acknowledgments: The authors thank the Ministry of Higher Education of Malaysia and the Center for Research and Instrumentation (CRIM) UKM and the laboratory assistants at UKM for their collaboration during instrumental analysis and the chemicals supplied.

Conflicts of Interest: The authors declare no conflict of interest.

References

1. Chaturvedi, S.; Dave, P.N.; Shah, N. Applications of nano-catalyst in new era. *J. Saudi Chem. Soc.* **2012**, *16*, 30N7–325. [[CrossRef](#)]
2. Kotha, S.S.; Sharma, N.; Sekar, G. An Efficient, Stable and Reusable Palladium Nanocatalyst: Chemoselective Reduction of Aldehydes with Molecular Hydrogen in Water. *Adv. Synth. Catal.* **2016**, *358*, 1694–1698. [[CrossRef](#)]
3. Mahmoud, M.A.; El-Sayed, M.A. Enhancing Catalytic Efficiency of Hollow Palladium Nanoparticles by Photothermal Heating of Gold Nanoparticles Added to the Cavity: Palladium–Gold Nanorattles. *ChemCatChem* **2014**, *6*, 3540–3546. [[CrossRef](#)]
4. Hu, C.; Yang, C.; Wang, X.; Wang, X.; Zhen, S.; Zhan, L.; Huang, C.; Li, Y. Rapid and facile synthesis of Au nanoparticle-decorated porous MOFs for the efficient reduction of 4-nitrophenol. *Sep. Purif. Technol.* **2022**, *300*, 121801. [[CrossRef](#)]
5. Taheri-Ledari, R.; Mirmohammadi, S.S.; Valadi, K.; Maleki, A.; Shalan, A.E. Convenient conversion of hazardous nitrobenzene derivatives to aniline analogues by Ag nanoparticles, stabilized on a naturally magnetic pumice/chitosan substrate. *RSC Adv.* **2020**, *10*, 43670–43681. [[CrossRef](#)] [[PubMed](#)]
6. Chun, Y.S.; Shin, J.Y.; Song, C.E.; Lee, S.-G. Palladium nanoparticles supported onto ionic carbon nanotubes as robust recyclable catalysts in an ionic liquid. *Chem. Commun.* **2008**, *8*, 942–944. [[CrossRef](#)] [[PubMed](#)]
7. Guarnizo, A.; Angurell, I.; Muller, G.; Llorca, J.; Seco, M.; Rossell, O.; Rossell, M.D. Highly water-dispersible magnetite-supported Pd nanoparticles and single atoms as excellent catalysts for Suzuki and hydrogenation reactions. *RSC Adv.* **2016**, *6*, 68675–68684. [[CrossRef](#)]
8. Santra, S.; Ranjan, P.; Bera, P.; Ghosh, P.; Mandal, S.K. Anchored palladium nanoparticles onto single walled carbon nanotubes: Efficient recyclable catalyst for N-containing heterocycles. *RSC Adv.* **2012**, *2*, 7523–7533. [[CrossRef](#)]
9. Shin, J.Y.; Lee, B.S.; Jung, Y.; Kim, S.J.; Lee, S.-G. Palladium nanoparticles captured onto spherical silica particles using a urea cross-linked imidazolium molecular band. *Chem. Commun.* **2007**, *48*, 5238–5240. [[CrossRef](#)]
10. Wang, Y.; Liu, J.; Wang, P.; Werth, C.J.; Strathmann, T.J. Palladium nanoparticles encapsulated in core–shell silica: A structured hydrogenation catalyst with enhanced activity for reduction of oxyanion water pollutants. *ACS Catal.* **2014**, *4*, 3551–3559. [[CrossRef](#)]
11. Huang, X.H.; Moon, B.K.; Byeon, S.J.; Heo, M.S.; Kim, I. Palladium nanoparticles decorated mesoporous carbon spheres as catalyst for reduction of 4-nitrophenol. *J. Nanosci. Nanotechnol.* **2014**, *14*, 8771–8776. [[CrossRef](#)] [[PubMed](#)]
12. Siamaki, A.R.; Lin, Y.; Woodberry, K.; Connell, J.W.; Gupton, B.F. Palladium nanoparticles supported on carbon nanotubes from solventless preparations: Versatile catalysts for ligand-free Suzuki cross coupling reactions. *J. Mater. Chem. A* **2013**, *1*, 12909–12918. [[CrossRef](#)]
13. Liew, K.H.; Loh, P.L.; Juan, J.C.; Yarmo, M.A.; Yusop, R.M. QuadraPure-supported palladium nanocatalysts for microwave-promoted Suzuki cross-coupling reaction under aerobic condition. *Sci. World J.* **2014**, *2014*, 796196. [[CrossRef](#)] [[PubMed](#)]
14. Liew, K.H.; Samad, W.Z.; Nordin, N.; Loh, P.L.; Juan, J.C.; Yarmo, M.A.; Yahaya, B.H.; Yusop, R.M. Preparation and characterization of HypoGel-supported Pd nanocatalysts for Suzuki reaction under mild conditions. *Chin. J. Catal.* **2015**, *36*, 771–777. [[CrossRef](#)]
15. Najman, R.; Cho, J.K.; Coffey, A.F.; Davies, J.W.; Bradley, M. Entangled palladium nanoparticles in resin plugs. *Chem. Commun.* **2007**, *47*, 5031–5033. [[CrossRef](#)] [[PubMed](#)]

16. Sargin, I.; Baran, T.; Arslan, G. Environmental remediation by chitosan-carbon nanotube supported palladium nanoparticles: Conversion of toxic nitroarenes into aromatic amines, degradation of dye pollutants and green synthesis of biaryls. *Sep. Purif. Technol.* **2020**, *247*, 116987. [[CrossRef](#)]
17. Nasrollahzadeh, M.; Jaleh, B.; Baran, T.; Varma, R.S. Efficient degradation of environmental contaminants using Pd-RGO nanocomposite as a retrievable catalyst. *Clean Technol. Environ. Policy* **2020**, *22*, 325–335. [[CrossRef](#)]
18. Luo, W.; Luo, K.; Yang, Y.; Lin, X.; Li, P.; Wen, Y. N-maleyl chitosan-supported palladium catalyst for Heck coupling reaction and reduction of 4-nitrophenol. *Colloids Surf. A Physicochem. Eng. Asp.* **2022**, *652*, 129852. [[CrossRef](#)]
19. Akbayrak, S.; Kaya, M.; Volkan, M.; Özkaz, S. Palladium (0) nanoparticles supported on silica-coated cobalt ferrite: A highly active, magnetically isolable and reusable catalyst for hydrolytic dehydrogenation of ammonia borane. *Appl. Catal. B Environ.* **2014**, *147*, 387–393. [[CrossRef](#)]
20. Qiu, Y.; Ma, Z.; Hu, P. Environmentally benign magnetic chitosan/Fe₃O₄ composites as reductant and stabilizer for anchoring Au NPs and their catalytic reduction of 4-nitrophenol. *J. Mater. Chem. A* **2014**, *2*, 13471–13478. [[CrossRef](#)]
21. Rahimi, J.; Taheri-Ledari, R.; Niksefat, M.; Maleki, A. Enhanced reduction of nitrobenzene derivatives: Effective strategy executed by Fe₃O₄/PVA-10%Ag as a versatile hybrid nanocatalyst. *Catal. Commun.* **2020**, *134*, 105850. [[CrossRef](#)]
22. Baykal, A.; Karaoglu, E.; Sözeri, H.; Uysal, E.; Toprak, M.S. Synthesis and characterization of high catalytic activity magnetic Fe₃O₄ supported Pd nanocatalyst. *J. Supercond. Nov. Magn.* **2013**, *26*, 165–171. [[CrossRef](#)]
23. Taheri-Ledari, R.; Rahimi, J.; Maleki, A.; Shalan, A.E. Ultrasound-assisted diversion of nitrobenzene derivatives to their aniline equivalents through a heterogeneous magnetic Ag/Fe₃O₄-IT nanocomposite catalyst. *New J. Chem.* **2020**, *44*, 19827–19835. [[CrossRef](#)]
24. Hassanzadeh-Afruzi, F.; Asgharnasl, S.; Mehraeen, S.; Amiri-Khamakani, Z.; Maleki, A. Guanidinylated SBA-15/Fe₃O₄ mesoporous nanocomposite as an efficient catalyst for the synthesis of pyranopyrazole derivatives. *Sci. Rep.* **2021**, *11*, 19852. [[CrossRef](#)]
25. Bahrami, S.; Hassanzadeh-Afruzi, F.; Maleki, A. Synthesis and characterization of a novel and green rod-like magnetic ZnS/CuFe₂O₄/agar organometallic hybrid catalyst for the synthesis of biologically-active 2-amino-tetrahydro-4H-chromene-3-carbonitrile derivatives. *Appl. Organomet. Chem.* **2020**, *34*, e5949. [[CrossRef](#)]
26. Fernandes, C.; Pereira, C.; Fernandez-Garcia, M.P.; Pereira, A.M.; Guedes, A.; Fernandez-Pacheco, R.; Ibarra, A.; Ibarra, M.R.; Araujo, J.P.; Freire, C. Tailored design of Co_xMn_{1-x}Fe₂O₄ nanoferrites: A new route for dual control of size and magnetic properties. *J. Mater. Chem. C* **2014**, *2*, 5818–5828. [[CrossRef](#)]
27. Xu, W.-H.; Wang, L.; Wang, J.; Sheng, G.-P.; Liu, J.-H.; Yu, H.-Q.; Huang, X.-J. Superparamagnetic mesoporous ferrite nanocrystal clusters for efficient removal of arsenite from water. *CrystEngComm* **2013**, *15*, 7895–7903. [[CrossRef](#)]
28. Rocha, M.; Fernandes, C.; Pereira, C.; Rebelo, S.L.; Pereira, M.F.; Freire, C. Gold-supported magnetically recyclable nanocatalysts: A sustainable solution for the reduction of 4-nitrophenol in water. *Rsc Adv.* **2015**, *5*, 5131–5141. [[CrossRef](#)]
29. Lu, A.H.; Salabas, E.e.L.; Schüth, F. Magnetic nanoparticles: Synthesis, protection, functionalization, and application. *Angew. Chem. Int. Ed.* **2007**, *46*, 1222–1244. [[CrossRef](#)]
30. Iqbal, Y.; Bae, H.; Rhee, I.; Hong, S. Magnetic heating of silica-coated manganese ferrite nanoparticles. *J. Magn. Magn. Mater.* **2016**, *409*, 80–86. [[CrossRef](#)]
31. Rufato, K.B.; Galdino, J.P.; Ody, K.S.; Pereira, A.G.; Corradini, E.; Martins, A.F.; Paulino, A.T.; Fajardo, A.R.; Aouada, F.A.; La Porta, F.A. Hydrogels based on chitosan and chitosan derivatives for biomedical applications. In *Hydrogels-Smart Materials for Biomedical Applications*; IntechOpen: London, UK, 2018.
32. de Oliveira Arias, J.L.; Schneider, A.; Batista-Andrade, J.A.; Vieira, A.A.; Caldas, S.S.; Primel, E.G. Chitosan from shrimp shells: A renewable sorbent applied to the clean-up step of the QuEChERS method in order to determine multi-residues of veterinary drugs in different types of milk. *Food Chem.* **2018**, *240*, 1243–1253. [[CrossRef](#)] [[PubMed](#)]
33. Lee, M.; Chen, B.-Y.; Den, W. Chitosan as a natural polymer for heterogeneous catalysts support: A short review on its applications. *Appl. Sci.* **2015**, *5*, 1272–1283. [[CrossRef](#)]
34. Dabbawala, A.A.; Sudheesh, N.; Bajaj, H.C. Palladium supported on chitosan as a recyclable and selective catalyst for the synthesis of 2-phenyl ethanol. *Dalton Trans.* **2012**, *41*, 2910–2917. [[CrossRef](#)]
35. Baig, R.N.; Nadagouda, M.N.; Varma, R.S. Ruthenium on chitosan: A recyclable heterogeneous catalyst for aqueous hydration of nitriles to amides. *Green Chem.* **2014**, *16*, 2122–2127. [[CrossRef](#)]
36. Baig, R.N.; Varma, R.S. Copper on chitosan: A recyclable heterogeneous catalyst for azide-alkyne cycloaddition reactions in water. *Green Chem.* **2013**, *15*, 1839–1843. [[CrossRef](#)]
37. de Souza, J.F.; da Silva, G.T.; Fajardo, A.R. Chitosan-based film supported copper nanoparticles: A potential and reusable catalyst for the reduction of aromatic nitro compounds. *Carbohydr. Polym.* **2017**, *161*, 187–196. [[CrossRef](#)]
38. Chen, X.; Yang, H.; Yan, N. Shell biorefinery: Dream or reality? *Chem.—A Eur. J.* **2016**, *22*, 13402–13421. [[CrossRef](#)]
39. Thorat, N.; Otari, S.; Patil, R.; Bohara, R.; Yadav, H.; Koli, V.; Chaurasia, A.; Ningthoujam, R. Synthesis, characterization and biocompatibility of chitosan functionalized superparamagnetic nanoparticles for heat activated curing of cancer cells. *Dalton Trans.* **2014**, *43*, 17343–17351. [[CrossRef](#)]
40. Streu, C.; Meggers, E. Ruthenium-induced allylcarbamate cleavage in living cells. *Angew. Chem. Int. Ed.* **2006**, *45*, 5645–5648. [[CrossRef](#)]
41. Yusop, R.M.; Unciti-Broceta, A.; Johansson, E.; Sánchez-Martín, R.M.; Bradley, M. Palladium-mediated intracellular chemistry. *Nat. Chem.* **2011**, *3*, 239–243. [[CrossRef](#)]

42. Kamalzare, M.; Ahghari, M.R.; Bayat, M.; Maleki, A. Fe₃O₄@chitosan-tannic acid bionanocomposite as a novel nanocatalyst for the synthesis of pyranopyrazoles. *Sci. Rep.* **2021**, *11*, 20021. [[CrossRef](#)] [[PubMed](#)]
43. Kamalzare, M.; Bayat, M.; Maleki, A. Green and efficient three-component synthesis of 4H-pyran catalysed by CuFe₂O₄@starch as a magnetically recyclable bionanocatalyst. *R. Soc. Open Sci.* **2020**, *7*, 200385. [[CrossRef](#)]
44. Dell'Anna, M.M.; Intini, S.; Romanazzi, G.; Rizzuti, A.; Leonelli, C.; Piccinni, F.; Mastroilli, P. Polymer supported palladium nanocrystals as efficient and recyclable catalyst for the reduction of nitroarenes to anilines under mild conditions in water. *J. Mol. Catal. A Chem.* **2014**, *395*, 307–314. [[CrossRef](#)]
45. Vincent, T.; Peirano, F.; Guibal, E. Chitosan supported palladium catalyst. VI. Nitroaniline degradation. *J. Appl. Polym. Sci.* **2004**, *94*, 1634–1642. [[CrossRef](#)]
46. Ai, L.; Jiang, J. Catalytic reduction of 4-nitrophenol by silver nanoparticles stabilized on environmentally benign macroscopic biopolymer hydrogel. *Bioresour. Technol.* **2013**, *132*, 374–377. [[CrossRef](#)]
47. Zheng, Y.; Zhu, Y.; Tian, G.; Wang, A. In situ generation of silver nanoparticles within crosslinked 3D guar gum networks for catalytic reduction. *Int. J. Biol. Macromol.* **2015**, *73*, 39–44. [[CrossRef](#)]
48. Silambarasan, S.; Vangnai, A.S. Biodegradation of 4-nitroaniline by plant-growth promoting *Acinetobacter* sp. AVLB2 and toxicological analysis of its biodegradation metabolites. *J. Hazard. Mater.* **2016**, *302*, 426–436. [[CrossRef](#)]
49. Shen, H.; Gao, J.; Wang, J. Assessment of toxicity of two nitroaromatic compounds in the freshwater fish *Cyprinus carpio*. *Front. Environ. Sci. Eng.* **2012**, *6*, 518–523. [[CrossRef](#)]
50. Wu, W.; Liu, G.; Liang, S.; Chen, Y.; Shen, L.; Zheng, H.; Yuan, R.; Hou, Y.; Wu, L. Efficient visible-light-induced photocatalytic reduction of 4-nitroaniline to p-phenylenediamine over nanocrystalline PbBi₂Nb₂O₉. *J. Catal.* **2012**, *290*, 13–17. [[CrossRef](#)]
51. Trivedi, M.K.; Branton, A.; Trivedi, D.; Nayak, G.; Singh, R.; Jana, S. Characterization of physical, thermal and spectroscopic properties of biofield energy treated p-phenylenediamine and p-toluidine. *Environ. Anal. Toxicol.* **2015**, *5*, 1–10.
52. Ikarashi, Y.; Kaniwa, M.-A. Determination of p-Phenylenediamine and Related Antioxidants in Rubber Boots by High Performance Liquid Chromatography. Development of an Analytical Method for N-(1-Methylheptyl)-N'-phenyl-p-phenylenediamine. *J. Health Sci.* **2000**, *46*, 467–473. [[CrossRef](#)]
53. Robert, A. Phenyleneand Toluenediamines. In *Ullmann's Encyclopedia of Industrial Chemistry*; Verlag Chemie: Hoboken, NJ, USA, 2002.
54. Beugelmans, R.; Neuville, L.; Bois-Choussy, M.; Chastanet, J.; Zhu, J. Palladium catalyzed reductive deprotection of alloc: Transprotection and peptide bond formation. *Tetrahedron Lett.* **1995**, *36*, 3129–3132. [[CrossRef](#)]
55. Franco, D.; Duñach, E. New and mild allyl carbamate deprotection method catalyzed by electrogenerated nickel complexes. *Tetrahedron Lett.* **2000**, *41*, 7333–7336. [[CrossRef](#)]
56. Vutukuri, D.R.; Bharathi, P.; Yu, Z.; Rajasekaran, K.; Tran, M.-H.; Thayumanavan, S. A mild deprotection strategy for allyl-protecting groups and its implications in sequence specific dendrimer synthesis. *J. Org. Chem.* **2003**, *68*, 1146–1149. [[CrossRef](#)] [[PubMed](#)]
57. Pereira, C.; Pereira, A.M.; Fernandes, C.; Rocha, M.; Mendes, R.; Fernández-García, M.P.; Guedes, A.; Tavares, P.B.; Grenèche, J.-M.; Araújo, J.o.P. Superparamagnetic MFe₂O₄ (M= Fe, Co, Mn) nanoparticles: Tuning the particle size and magnetic properties through a novel one-step coprecipitation route. *Chem. Mater.* **2012**, *24*, 1496–1504. [[CrossRef](#)]
58. Liew, K.H.; Lee, T.K.; Yarmo, M.A.; Loh, K.S.; Peixoto, A.F.; Freire, C.; Yusop, R.M. Ruthenium Supported on Ionically Cross-linked Chitosan-Carrageenan Hybrid MnFe₂O₄ Catalysts for 4-Nitrophenol Reduction. *Catalysts* **2019**, *9*, 254. [[CrossRef](#)]
59. Chauhan, S. Modification of chitosan for sorption of metal ions. *J. Chem. Pharm. Res.* **2015**, *7*, 49–55.
60. Kołodziejczak-Radzimska, A.; Markiewicz, E.; Jesionowski, T. Structural characterisation of ZnO particles obtained by the emulsion precipitation method. *J. Nanomater.* **2012**, *2012*, 15. [[CrossRef](#)]
61. Rivas, P.; Sagredo, V.; Rossi, F.; Pernechele, C.; Solzi, M.; Peña, O. Structural, magnetic, and optical characterization of MnFe₂O₄ nanoparticles synthesized via sol-gel method. *IEEE Trans. Magn.* **2013**, *49*, 4568–4571. [[CrossRef](#)]
62. Yang, L.-X.; Wang, F.; Meng, Y.-F.; Tang, Q.-H.; Liu, Z.-Q. Fabrication and characterization of manganese ferrite nanospheres as a magnetic adsorbent of chromium. *J. Nanomater.* **2013**, *2013*, 2. [[CrossRef](#)]
63. Heinrich, F.; Keßler, M.T.; Dohmen, S.; Singh, M.; Prechtel, M.H.; Mathur, S. Molecular palladium precursors for Pd⁰ nanoparticle preparation by microwave irradiation: Synthesis, structural characterization and catalytic activity. *Eur. J. Inorg. Chem.* **2012**, *2012*, 6027–6033. [[CrossRef](#)]
64. Kumari, S.; Layek, S.; Pathak, D.D. Palladium nanoparticles immobilized on a magnetic chitosan-anchored Schiff base: Applications in Suzuki–Miyaura and Heck–Mizoroki coupling reactions. *New J. Chem.* **2017**, *41*, 5595–5604.
65. Ruiz-Caro, R.; Veiga-Ochoa, M.D. Characterization and dissolution study of chitosan freeze-dried systems for drug controlled release. *Molecules* **2009**, *14*, 4370–4386. [[CrossRef](#)] [[PubMed](#)]
66. Reddy, G.K.; Ling, C.; Peck, T.C.; Jia, H. Understanding the chemical state of palladium during the direct NO decomposition— influence of pretreatment environment and reaction temperature. *RSC Adv.* **2017**, *7*, 19645–19655. [[CrossRef](#)]
67. Veisi, H.; Najafi, S.; Hemmati, S. Pd (II)/Pd (0) anchored to magnetic nanoparticles (Fe₃O₄) modified with biguanidine-chitosan polymer as a novel nanocatalyst for Suzuki–Miyaura coupling reactions. *Int. J. Biol. Macromol.* **2018**, *113*, 186–194. [[CrossRef](#)]
68. Zhao, C.; Zhang, Z.; Liu, Y.; Shang, N.; Wang, H.-J.; Wang, C.; Gao, Y. Palladium nanoparticles anchored on sustainable chitin for phenol hydrogenation to cyclohexanone. *ACS Sustain. Chem. Eng.* **2020**, *8*, 12304–12312. [[CrossRef](#)]

69. Sanchez-Ramirez, J.; Martinez-Hernandez, J.L.; Segura-Ceniceros, P.; Lopez, G.; Saade, H.; Medina-Morales, M.A.; Ramos-González, R.; Aguilar, C.N.; Ilyina, A. Cellulases immobilization on chitosan-coated magnetic nanoparticles: Application for *Agave Atrovirens* lignocellulosic biomass hydrolysis. *Bioprocess Biosyst. Eng.* **2017**, *40*, 9–22. [[CrossRef](#)]
70. Kumar, S.; Koh, J. Physicochemical, optical and biological activity of chitosan-chromone derivative for biomedical applications. *Int. J. Mol. Sci.* **2012**, *13*, 6102–6116. [[CrossRef](#)]
71. Wang, X.; Chang, P.R.; Li, Z.; Wang, H.; Liang, H.; Cao, X.; Chen, Y. Chitosan-coated cellulose/soy protein membranes with improved physical properties and hemocompatibility. *BioResources* **2011**, *6*, 1392–1413.
72. Salah, T.A.; Mohammad, A.M.; Hassan, M.A.; El-Anadouli, B.E. Development of nano-hydroxyapatite/chitosan composite for cadmium ions removal in wastewater treatment. *J. Taiwan Inst. Chem. Eng.* **2014**, *45*, 1571–1577. [[CrossRef](#)]
73. Cordero-Arias, L.; Cabanas-Polo, S.; Gao, H.; Gilibert, J.; Sanchez, E.; Roether, J.; Schubert, D.; Virtanen, S.; Boccaccini, A.R. Electrophoretic deposition of nanostructured-TiO₂/chitosan composite coatings on stainless steel. *RSC Adv.* **2013**, *3*, 11247–11254. [[CrossRef](#)]
74. Bujňáková, Z.; Dutková, E.; Kello, M.; Mojžiš, J.; Baláž, M.; Baláž, P.; Shpotyuk, O. Mechanochemistry of chitosan-coated zinc sulfide (ZnS) nanocrystals for bio-imaging applications. *Nanoscale Res. Lett.* **2017**, *12*, 328. [[CrossRef](#)] [[PubMed](#)]
75. Sionkowska, A.; Planecka, A. Preparation and characterization of silk fibroin/chitosan composite sponges for tissue engineering. *J. Mol. Liq.* **2013**, *178*, 5–14. [[CrossRef](#)]
76. Mpungose, P.P.; Vundla, Z.P.; Maguire, G.E.; Friedrich, H.B. The current status of heterogeneous palladium catalysed Heck and Suzuki cross-coupling reactions. *Molecules* **2018**, *23*, 1676. [[CrossRef](#)]
77. Pagliaro, M.; Pandarus, V.; Beland, F.; Ciriminna, R.; Palmisano, G.; Cara, P.D. A new class of heterogeneous Pd catalysts for synthetic organic chemistry. *Catal. Sci. Technol.* **2011**, *1*, 736–739. [[CrossRef](#)]
78. Rashad, M.M. Magnetic properties of nanocrystalline magnesium ferrite by co-precipitation assisted with ultrasound irradiation. *J. Mater. Sci.* **2007**, *42*, 5248–5255. [[CrossRef](#)]
79. Unsoy, G.; Yalcin, S.; Khodadust, R.; Gunduz, G.; Gunduz, U. Synthesis optimization and characterization of chitosan-coated iron oxide nanoparticles produced for biomedical applications. *J. Nanoparticle Res.* **2012**, *14*, 964. [[CrossRef](#)]
80. Le, X.; Dong, Z.; Liu, Y.; Jin, Z.; Huy, T.-D.; Le, M.; Ma, J. Palladium nanoparticles immobilized on core-shell magnetic fibers as a highly efficient and recyclable heterogeneous catalyst for the reduction of 4-nitrophenol and Suzuki coupling reactions. *J. Mater. Chem. A* **2014**, *2*, 19696–19706. [[CrossRef](#)]
81. Babji, P.S.; Rao, V.L. Catalytic reduction of 4-Nitrophenol to 4-Aminophenol by using Fe₂O₃-Cu₂O-TiO₂ nanocomposite. *Int. J. Chem. Stud.* **2016**, *4*, 123–127.
82. Lee, J.H.; Hong, S.K.; Ko, W.B. Reduction of 4-Nitrophenol Catalyzed by Platinum Nanoparticles Embedded into Carbon Nanocolloids. *Asian J. Chem.* **2011**, *23*, 2347–2350.
83. Kurtan, U.; Amir, M.; Baykal, A. A Fe₃O₄@Nico@Ag nanocatalyst for the hydrogenation of nitroaromatics. *Chin. J. Catal.* **2015**, *36*, 705–711. [[CrossRef](#)]
84. Noschese, A.; Buonerba, A.; Canton, P.; Milione, S.; Capacchione, C.; Grassi, A. Highly efficient and selective reduction of nitroarenes into anilines catalyzed by gold nanoparticles incarcerated in a nanoporous polymer matrix: Role of the polymeric support and insight into the reaction mechanism. *J. Catal.* **2016**, *340*, 30–40. [[CrossRef](#)]
85. Bhattacharjee, D.; Mandal, K.; Dasgupta, S. Hydrazine assisted catalytic hydrogenation of PNP to PAP by Ni_xPd_{100-x} nanocatalyst. *RSC Adv.* **2016**, *6*, 64364–64373. [[CrossRef](#)]
86. Zhang, D.; Xu, N.; Li, H.; Yao, Q.; Xu, F.; Fan, J.; Du, J.; Peng, X. Probing thiophenol pollutant in solutions and cells with BODIPY-based fluorescent probe. *Ind. Eng. Chem. Res.* **2017**, *56*, 9303–9309. [[CrossRef](#)]
87. Dumont, J.; Euwart, D.; Mei, B.; Estes, S.; Kshirsagar, R. Human cell lines for biopharmaceutical manufacturing: History, status, and future perspectives. *Crit. Rev. Biotechnol.* **2016**, *36*, 1110–1122. [[CrossRef](#)]

Disclaimer/Publisher's Note: The statements, opinions and data contained in all publications are solely those of the individual author(s) and contributor(s) and not of MDPI and/or the editor(s). MDPI and/or the editor(s) disclaim responsibility for any injury to people or property resulting from any ideas, methods, instructions or products referred to in the content.